**Earthline Journal of Chemical Sciences**
E-ISSN: 2581-9003; CODEN: EJCSB4
Volume 13, Number 3, August 2026, Pages 341-355
https://doi.org/10.34198/ejcs.13326.24.341355

# Hydrogen peroxide oxidation of native starches from different biomass sources: Kinetic, structural and thermal study

**Ouattara Taniky Sy Hamed**

Laboratoire de Thermodynamique et de Physico-Chimie du Milieu, Université Nangui ABROGOUA, 02 BP 802 Abidjan 02, Côte d'Ivoire

**Yacouba Zoungranan***

Laboratoire de Thermodynamique et de Physico-Chimie du Milieu, Université Nangui ABROGOUA, 02 BP 802 Abidjan 02, Côte d'Ivoire

Département de Mathématiques Physique Chimie, Université Peleforo GON COULIBALY, B.P. 1328, Korhogo, Côte d'Ivoire
e-mail: zoungranan@gmail.com

**Ekou Lynda**

Laboratoire de Thermodynamique et de Physico-Chimie du Milieu, Université Nangui ABROGOUA, 02 BP 802 Abidjan 02, Côte d'Ivoire

**Ekou Tchirioua**

Laboratoire de Thermodynamique et de Physico-Chimie du Milieu, Université Nangui ABROGOUA, 02 BP 802 Abidjan 02, Côte d'Ivoire

**Kaga Taba To'ora**

Laboratoire de l'Eau et de l'Environnement de Limoges (E2Lim), UR 24133, ENSIL-ENSCI, Université de Limoges, France

## Abstract

Starch is a natural, renewable, economical, and widely available polymer used as a gelling agent, thickener, binder, and potential raw material in many food products. Due to its techno-functional properties, the food and non-food industries are interested in developing starch-based materials such as films, hydrogels, starch nanoparticles, and other derivatives. This study focused on the kinetics of hydrogen peroxide oxidation of starches from four biomass sources (Yam, Cor, Pot, and Cas), as well as their structural and thermal properties. The results show that, for all the starches studied, the oxidation process is adequately described by pseudo-first-order kinetics. The crystallinity indices obtained are 27.071 ± 0.24%, 30.226 ± 0.30%, 41.170 ± 0.45%, and 36.413 ± 0.34% for Cas, Pot, Cor, and Yam, respectively. The TGA/DTG analysis highlights three phases of thermal degradation: the first is linked to the loss of residual moisture below 100°C, followed by major degradation between 150 and 310°C associated with the breakdown of glycosidic bonds. A third phase, between 310 and 550°C, is associated with the carbonization of residues, with the differences observed between starches reflecting the influence of botanical origin and structural composition on their thermal stability.

Received: July 23, 2026; Revised & Accepted: August 18, 2026; Published online: August 25, 2026

Keywords and phrases: native starch, hydrogen peroxide, starch oxidation, oxidation kinetics, pseudo-order kinetics, biomass sources.

*Corresponding author

**Graphical Abstract**

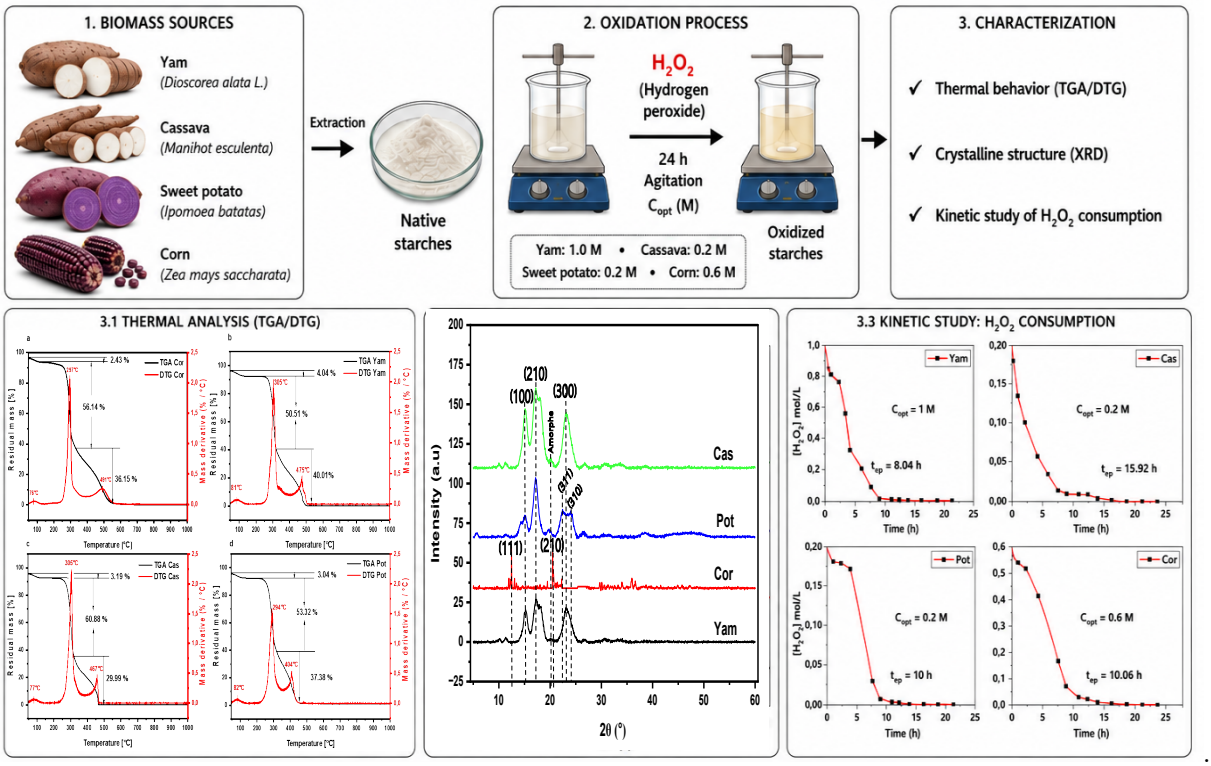


## 1. Introduction

Starch is a natural biopolymer that is attracting growing interest in food and non-food applications [1]. It is mainly composed of amylose and amylopectin. Amylose has a linear α-(1→4)-D-glucopyranose chain structure, while amylopectin has a branched α-(1→6) chain structure [2]. The relative proportion of these two components varies from one starch to another and determines certain physicochemical properties such as gelation, viscosity, and thermal stability. Starch can be obtained directly from many agricultural biomasses such as cereals, tubers, legumes, and certain fruits [3]. The applications of starch in the non-food industrial sector range from paper production to the production of biodegradable plastics, including the pharmaceutical, cosmetics, and textile industries [4]. Although native starch is suitable for most industrial applications, in some cases it has limitations, including sensitivity to variations in temperature and pH, and low hydrophobicity. To meet certain specific needs, chemical, physical, or enzymatic modification of native starch is sometimes necessary. The aim of modification is to improve the structural and functional properties of native starch. Starch oxidation is a chemical modification that transforms the methyl hydroxyl groups of starch into carbonyl and carboxyl groups, thereby modifying its polarity, molar mass, and supramolecular organization. These changes directly affect the diffusivity of water and oxidizing agent molecules in the granules, resulting in a decrease in viscosity at constant shear, a change in rheological behavior, and a modification of the glass transition temperature ($T_g$), cold crystallization temperature ($T_c$), and melting temperature ($T_{fus}$) [5]. Among the existing chemical treatments, the oxidation of native starch by hydrogen peroxide stands out for its green credentials. This is because the oxidizing agent does not cause the production of toxic by-products in the oxidation reaction. In the process of modifying native starch by oxidation, the kinetics of the reaction can be studied by monitoring changes in the concentration of the oxidizing agent. Understanding the mechanisms of oxidation requires an in-depth kinetic study. However, monitoring $H_2O_2$ consumption makes it possible to determine the reaction order,

the rate constant (k), and the half-life ($t_{1/2/2}$), which reveal the interactions between hydroxyl radicals and reactive sites in starch. Most existing work on the chemical modification of starch focuses on the end products, without correlating the kinetics of the reaction with the structural and functional modifications of the oxidized starch obtained. However, these modifications provide insight into the thermo-rheological properties of oxidized starch. Chemical modification by controlled oxidation also significantly reduces the enthalpies of fusion and crystallinity [6]. In this study, the oxidation kinetics of four types of starches from various agricultural biomasses will be investigated. Thermal characterization, performed by TGA/DTG analysis, will be used to evaluate the thermal behavior of the four types of native starches studied. This analysis aims to identify the different stages of thermal degradation, estimate the associated mass losses, and compare the thermal stability of the starches according to their botanical origin.

## 2. Materials and Methods

### 2.1. Oxidation of native starches

In our previous work [7], tubers of yam (*Dioscorea alata L.*), sweet potato (*Ipomoea batatas*), cassava (*Manihot esculenta Crantz*), and corn kernels (*Zea mays saccharata*) were used to obtain native starches. The native starches from yams, sweet potatoes, cassava, and corn were designated Yam, Pot, Cas, and Cor, respectively. These starches were then oxidized with various concentrations of hydrogen peroxide. Optimal oxidation was achieved with hydrogen peroxide concentrations ($C_{opt}$) of 1M, 0.2M, 0.2M, and 0.6M $H_2O_2$, respectively. In this study, each oxidation test with a given starch will be performed with a hydrogen peroxide concentration ($C_{opt}$).

### 2.2. Characterization tests on native starches

#### TGA analysis

The thermal behavior of native starches was evaluated using an apparatus (Mettler Toledo TGA/DSC, Canada 2915 Argentia Road, Unit 6, Mississauga L5N 8G6), with a temperature range of 25 to 1000°C under air flow (80 mL.min$^{-1}$) and a heating gradient of 5°C/ min$^{-1}$.

#### Physicochemical characterization of native starches

The physicochemical parameters of native starches required for this study were established in previous work [7].

#### Structural analysis

X-ray diffraction was used to determine the crystallinity of native starches. The samples were analyzed using an X-ray diffractometer (D8-advance Bruker AXS GmbH, Karlsruhe (Germany)) at room temperature with a monochromatic Cu kα radiation source (λ = 0.1539 nm) in step scanning mode with an angle 2Θ ranging from 10º to 60º and a scanning time of 5 min. The crystallinity index ($C_rI$) was determined using Ségale's empirical method [8,9].

$$C_rI\ (\%) = \frac{I_{cris} - I_{amor}}{I_{cris}} \times 100 \quad (1)$$

With $I_{cris}$ and $I_{amor}$ representing the maximum intensities in the crystalline and amorphous regions of the valley between two crystalline planes, respectively.

### 2.3. General methodology of the kinetic study

#### 2.3.1. Hydrogen peroxide calibration curve

A 0.02 M hydrogen peroxide ($H_2O_2$) stock solution was prepared from a commercially available 50% concentrated solution. This stock solution was diluted to obtain a series of solutions with concentrations $C_i$ equal to $1.10^{-3}$ M, $2.10^{-3}$ M, $3.10^{-3}$ M, $4.10^{-3}$ M, and $5.10^{-3}$ M, respectively. The experiment was carried out in five (5) 10 mL tubes. In each tube, a variable volume of $H_2O_2$ was introduced, ranging from 0.5 mL to 2.5 mL in increments of 0.5 mL. To these volumes, 1 mL of 0.1 M KI solution and 1 mL of 0.01 M $H_2SO_4$ solution were added successively. The redox reaction between hydrogen peroxide, potassium iodide (KI), and sulfuric acid ($H_2SO_4$) leads to the formation of diiodine ($I_2$), which serves as an indicator of the progress of the reaction. The tubes containing the mixtures were cooled in an ice bath for 5 minutes before determining the optical density. The resulting calibration curve is shown in Figure 1.

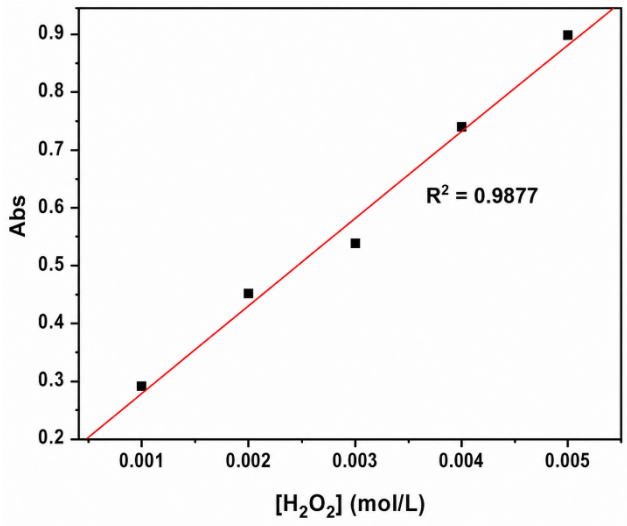


**Figure 1.** Calibration curve.

#### 2.3.2. Kinetic study of oxidation

For a given native starch, the kinetic study was carried out using a series of eight beakers labeled according to different stirring times: $t_i$ = 40 min, 1 h, 2 h, 4 h, 8 h, 10 h, 12 h, 16 h, 18 h, 20 h, 22 h, and 24 h. In each beaker, 5 g of native starch was added, followed by 25 mL of hydrogen peroxide ($H_2O_2$) at ($C_{opt}$). The mixture was stirred at 60 rpm using an orbital shaker (Innova 2300 Shaker, Germany). At the end of the stirring time, the beaker is removed and the starch solution is filtered under gravity using a Whatman No. 4 filter. A volume of 4 mL of the filtrate is collected in a tube, then 1 mL of $H_2SO_4$ and 5 mL of a 0.1 M potassium iodide (KI) solution are added successively. The optical density of the solution obtained is read using a dual-beam UV-Visible spectrophotometer (Parie, France) at 320 nm. The residual concentration of $H_2O_2$ is then determined using the hydrogen peroxide calibration curve.

#### 2.3.3. Pseudo-order kinetics of the reaction

The study of the decomposition kinetics of hydrogen peroxide is a complex process that can be described using pseudo-order kinetic models. The residual concentrations of $H_2O_2$ were determined from the calibration curve after measuring the optical density of each solution. The concentrations obtained at different time points were then used to analyze the evolution of $H_2O_2$ consumption. The experimental data were fitted to three kinetic

models: pseudo-order 0, pseudo-order 1, and pseudo-order 2. These models made it possible to determine the corresponding kinetic parameters and to evaluate the quality of the fits based on the coefficient of determination ($R^2$). The integrated equations used for these three models are presented in Table 1.

**Table 1.** Pseudo-order kinetics models from the study

| Kinetics | Integrated equations | Parameters |
|---|---|---|
| **Pseudo-order 0** | $[A]_t = [A]_{0_{th}} - k_0 t$ | $k_0$ = apparent rate constant (mol·L$^{-1}$·h$^{-1}$)<br>$A_{0th}$ = theoretical initial concentration of $H_2O_2$ |
| **Pseudo-order 1** | $\ln[A]_t = ln[A]_{0th} - k_1 t$ | $k_1$ = apparent rate constant (h$^{-1}$)<br>$A_{0th}$ = theoretical initial concentration of $H_2O_2$ |
| **Pseudo-order 2** | $\frac{1}{[A]_t} = \frac{1}{[A]_{0th}} + k_2 t$ | $k_2$ = apparent rate constant (L·mol$^{-1}$·h$^{-1}$)<br>$A_{0th}$ = theoretical initial concentration of $H_2O_2$ |

The linear regression curve for each equation provides access to the theoretical kinetic parameters and allows the pseudo-reaction order to be deduced. The kinetics monitored are those for which the linear regression provides a high coefficient of determination and theoretical initial concentrations close to the experimental initial concentrations.

### 2.4. Data treatment

All calculations and graphs were performed using Origin Pro 2024. Mean values and standard deviation were determined from three individual measurements.

## 3. Results and Discussion

### 3.1. TGA/DTG analysis

The TGA/DTG curves for native starches are shown in Figure 2. Analysis of the thermal degradation of native starches reveals three main phases at the TGA level, resulting in three peaks at the DTG level.

The first phase is observed at temperatures below 100°C with a small loss of mass (< 5%) corresponding to the loss of residual moisture in the starches. This stage is mainly attributed to the evaporation of residual moisture trapped in the granular structure of the starches. In fact, water molecules weakly bound by hydrogen interactions to the hydroxyl groups of amylose and amylopectin are released during heating [10]. This water desorption manifests itself as exothermic transitions recorded at 76°C, 81°C, 77°C, and 82°C for corn starch (Cor) (Figure 2a), yam starch (Yam) (Figure 2b), cassava (Cas) (Figure 2c) and sweet potato (Pot) (Figure 2d). The small temperature differences between these peaks could be explained by minor differences in the structural organization and water retention capacity of the starches studied, linked to their botanical origin [11,12]. The second degradation phase occurs between 150°C and 310°C. It is observed in the temperature range for all types of starches. This stage constitutes the major degradation, with mass losses reaching 56.14% to 60.88% depending on the botanical origin. The DTG peak temperatures (297 to 305°C) for different starches correspond to the breaking of glycosidic bonds and the depolymerization of amylose and amylopectin. These results are consistent with previous reports indicating that the main pyrolysis of native starch generally occurs between 200 and 400°C, resulting in a significant release of volatile compounds [12]. The variation in intensity and temperature between different starch sources can be attributed to their amylose/amylopectin content, grain size, and degree of crystallinity, as previously reported by [13,14]. The third phase occurs in the temperature

range of 310°C–550°C for all starches and is associated with the carbonization of residual products and the final decomposition of refractory organic compounds. The DTG peaks observed (404–491°C) confirm this phenomenon. These results are comparable to those described by [15], who report that native starches undergo slow and progressive degradation of carbonaceous residues above 350°C. The marked differences between the samples (40.01% for Yam (Figure 2b) versus 37.38% for Pot (Figure 2d) reflect the disparities in thermal stability and structural composition of starches of different botanical origins. These variations (Table 2) corroborate the work of [16,17], which emphasizes that the thermal resistance of starches depends heavily on botanical nature and the relative proportion of amylose and amylopectin.

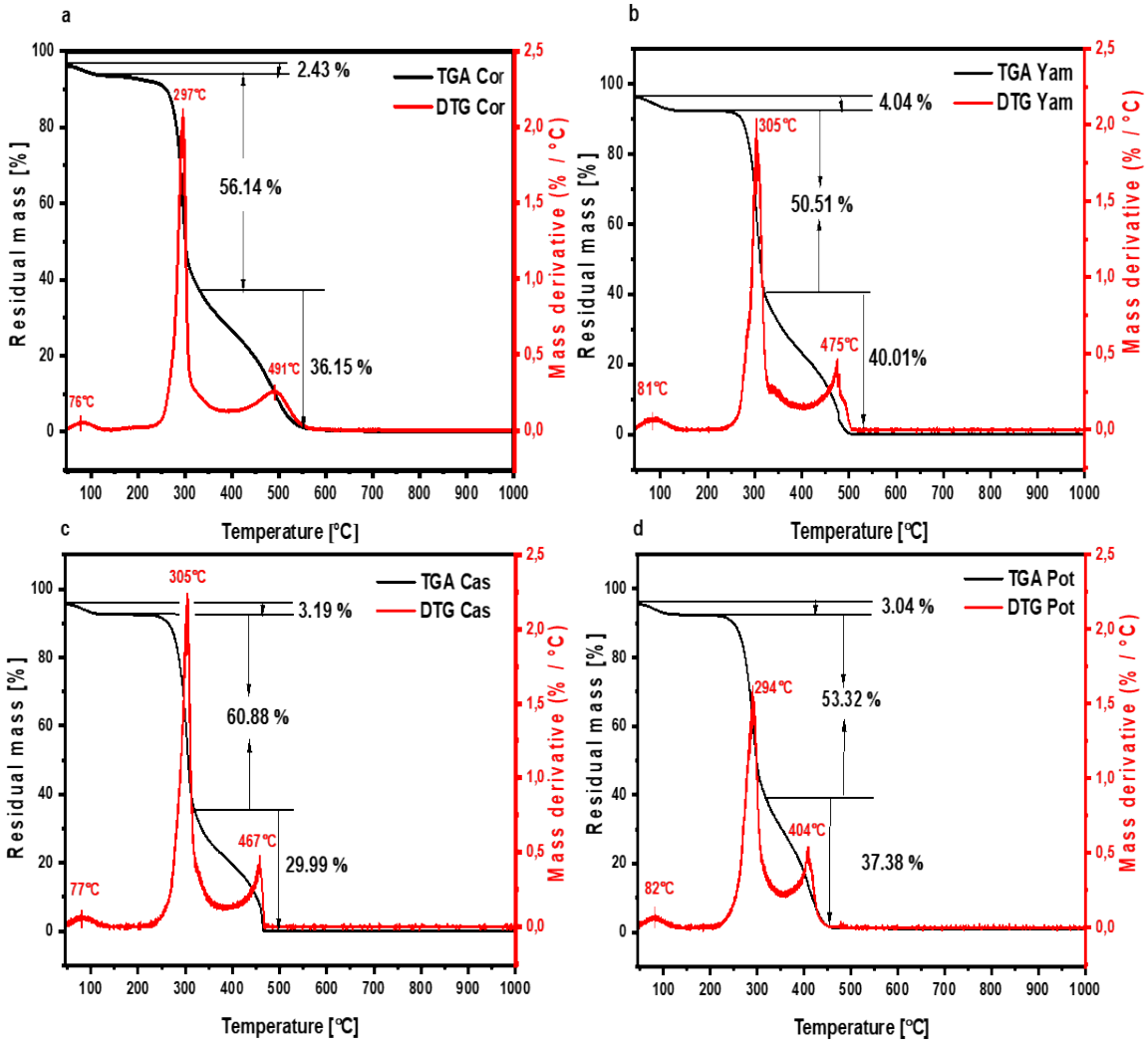


**Figure 2.** Thermogravimetric (TGA) and derivative thermogravimetric (DTG) curves of native starches recorded under an air atmosphere (flow rate: 80 mL $min^{-1}$) at a heating rate of 5 °C $min^{-1}$.

**Table 2.** Thermal degradation parameters of native starches determined by thermogravimetric analysis (TGA/DTG)

| Samples | Number of degradation phases | DTG peaks (°C) | Final residue (%) |
|---|---|---|---|
| Cor | 3 phases | 76 ± 1; 297 ± 2; 491 ± 3 | 5.28 ± 0.16 |
| Cas | 3 phases | 77 ± 1; 305 ± 3; 467 ± 4 | 5.94 ± 0.18 |
| Pot | 3 phases | 82 ± 2; 294 ± 3; 404 ± 3 | 6.26 ± 0.18 |
| Yam | 3 phases | 81 ± 2; 305 ± 3; 475 ± 4 | 4.44 ± 0.17 |

### 3.2. X-ray diffraction of starches

The diffractograms obtained from X-ray diffraction (XRD) analysis of native starches are shown in Figure 3. The XRD analyses made it possible to study the crystalline properties of the starches prior to treatment. The results highlight differences in crystalline organization depending on the botanical origin of the starches. These variations in crystallinity can influence the accessibility of reactive sites during oxidation by $H_2O_2$. Thus, XRD analysis provides structural information that complements the kinetic study.

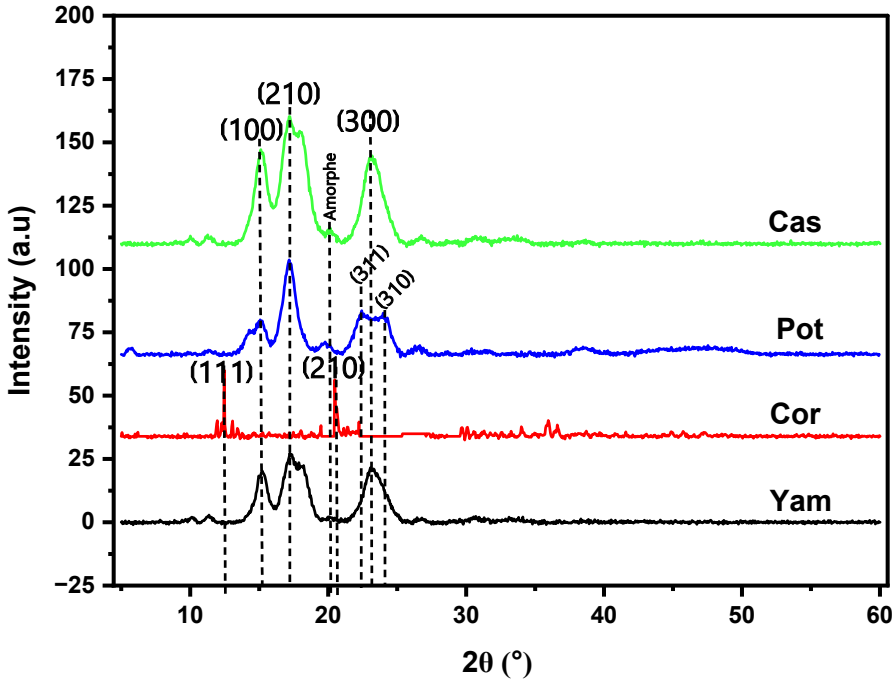


**Figure 3.** X-ray diffraction (XRD) patterns of native starches.

**Table 3.** Crystallinity index and interplanar spacing (d) of native starches determined by X-ray diffraction (XRD)

| Sample | Crystallinity index (%) | Crystalline type | d-spacing (Å) |
|---|---|---|---|
| Cas | 27.07 ± 0.24 | B | 5.86 ± 0.03; 5.15 ± 0.02; 3.84 ± 0.04 |
| Pot | 30.23 ± 0.30 | B | 5.86 ± 0.02; 5.15 ± 0.04; 3.97 ± 0.03; 3.70 ± 0.02 |
| Cor | 41.17 ± 0.45 | A | 7.13 ± 0.05; 4.34 ± 0.03 |
| Yam | 36.41 ± 0.34 | B | 5.86 ± 0.03; 5.15 ± 0.02; 3.84 ± 0.04 |

The starch diffractogram (Cor) reveals two intense peaks at 2θ = 12.42° and 20.47°, corresponding respectively to the (100) and (210) lattice planes. This type of peak is characteristic of type A starch, whose unit cell has orthorhombic symmetry [18]. Furthermore, the interplanar distance values suggest a compact, ordered structure, as is generally the case with cereal starches. This structure could explain the high crystallinity index observed (CI = 41.17 ± 0.45%). These results are consistent with previous studies. The starches (Cas, Yam, Pot) show multiple peaks between 2θ = 15° and 2θ = 24° for interplanar distances between (d = 3.70 ± 0.02Å -5.86 ± 0.03Å). These types of peaks are characteristic of type B starches, which have a hexagonal symmetry lattice.

These starches have a less dense and more irregular structure, with more amorphous regions that can retain water. This type of structure is characteristic of tuber starches. This structural organization therefore explains the low crystallinity index values obtained with these starches.

### 3.3. Kinetic study of the oxidation reaction

#### 3.3.1. Temporal evolution of $H_2O_2$ concentration

For a given concentration ($C_{opt}$), the residual concentrations of $H_2O_2$ were evaluated at various times over a 24 hour period. The results obtained are presented in Figure 4.

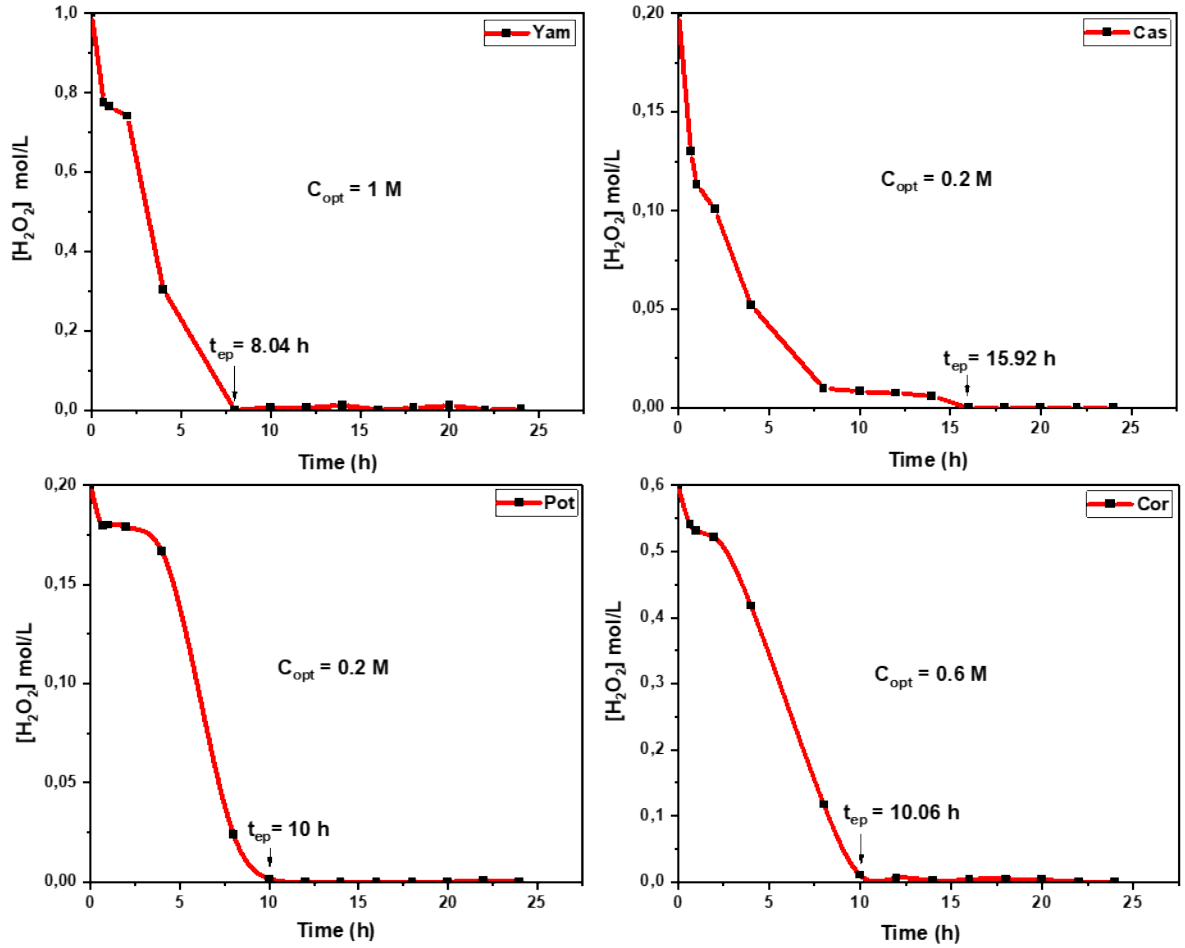


**Figure 4.** $H_2O_2$ consumption in native starches over 24 hours.

Analysis of Figure 4 shows that the residual $H_2O_2$ concentrations gradually decreased from their initial values ($C_{opt}$), reaching near-zero values at different depletion times ($t_{ep}$). The depletion time ($t_{ep}$, h) was defined as the time required for the residual $H_2O_2$ concentration to approach zero under the experimental conditions. The depletion times for the reactions with Pot, Cas, Yam, and Cor were 10.00, 15.92, 8.04, and 10.06 h, respectively. These differences in depletion time may be explained by a gradual decrease in readily accessible active sites and by diffusion limitations during the oxidation process. In addition, reaction intermediates and oxidized species formed during the reaction may induce competitive effects that slow down the $H_2O_2$ oxidation process. Kumoro et al. (2017) [19] also reported that, after surface oxidation, diffusion may become a limiting factor in the oxidation kinetics of polysaccharide matrices.For the same initial $H_2O_2$ concentration ($C_{opt}$ = 0.2 M), Pot reached near-complete depletion faster than Cas, with depletion times of 10.00 and 15.92h, respectively. Yam reached depletion after 8.04h despite having the highest initial $H_2O_2$ concentration ($C_{opt}$ = 1.0

M), whereas Cor required 10.06h at $C_{opt}$ = 0.6 M. To account for the differences in the initial $H_2O_2$ concentrations, the overall consumption behavior can be compared using the ratio $C_{opt}/t_{ep}$. The corresponding average consumption rates ($V= C_{opt}/t_{ep}$) were 0.1244, 0.0596, 0.0200, and 0.0126 M $h^{-1}$ for Yam, Cor, Pot, and Cas, respectively.Thus, the overall $H_2O_2$ consumption rates followed the order:

$$V_{Yam} > V_{Cor} > V_{Pot} > V_{Cas}$$

The higher overall consumption rate observed with Yam may be related to its relatively large accessible surface area and the availability of hydroxyl groups susceptible to oxidation. In addition, amylose-rich starches may expose a greater number of hydroxyl groups accessible to hydrogen peroxide oxidation, as previously reported by Zhou et al. (2016) [20]. The relatively low overall consumption rate observed with Cas cannot be attributed to a high degree of crystallinity, since Cas exhibited the lowest crystallinity index among the four starches (27.07 ± 0.24%), compared with 30.23 ± 0.30% for Pot, 36.41 ± 0.34% for Yam, and 41.17 ± 0.45% for Cor. Instead, this behavior may be related to its granular organization, relatively limited accessible surface area, differences in amylose/amylopectin composition, and diffusion limitations that may restrict the accessibility of reactive hydroxyl groups during the oxidation process.It should be noted that this overall consumption-rate ranking is distinct from the pseudo-first-order rate constants obtained from the kinetic regression analysis. The depletion time and the $C_{opt}/t_{ep}$ ratio describe the overall $H_2O_2$ consumption behavior, whereas $K_1$ represents an apparent kinetic parameter obtained from the pseudo-first-order model. Therefore, these parameters should be considered as complementary descriptors of the oxidation process rather than interchangeable measures of reaction rate.

### 3.3.2. Kinetic pseudo-orders

For each of the biomasses studied, the experimental data obtained from monitoring the temporal evolution of $H_2O_2$ were analyzed using various pseudo-order equations. Analysis of the corresponding linear regressions made it possible to determine the apparent order of the reaction.

### Pseudo-orders with Cor

For Cor starch, the linear regressions obtained are shown in Figure. 5 and the parameters of the various equations are listed in Table 4.

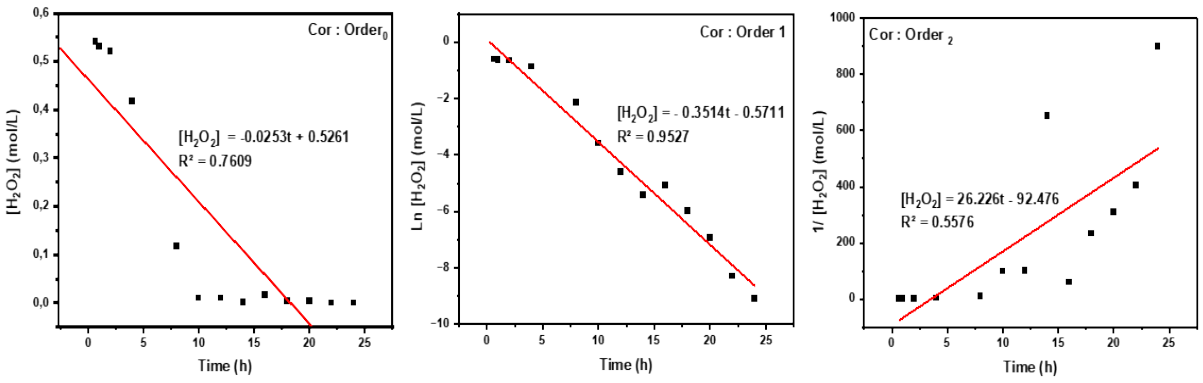


**Figure 5.** Reaction orders of starch oxidation reactions Cor.

**Table 4.** Kinetic parameters for $H_2O_2$ consumption by Cor biomass

| Order | Rate constant $k_i$ (i = 0, 1, 2) | Correlation coefficient $R^2$ | $[A]_{0th}$ (mol·L$^{-1}$) | $[A]_{0exp}$ (mol·L$^{-1}$) | Half-life $t_{1/2}$ (h) |
|---|---|---|---|---|---|
| **0** | 0.0253 ± 0.0012 mol·L$^{-1}$·h$^{-1}$ | 0.7609 ± 0.0123 | 0.5261 ± 0.0081 | 0.600 | 11.86 ± 0.44 |
| **1** | 0.351 ± 0.014 h$^{-1}$ | 0.9527 ± 0.0125 | 0.5649 ± 0.0129 | 0.600 | 1.973 ± 0.135 |
| **2** | 26.226 ± 1.42 L·mol$^{-1}$·h$^{-1}$ | 0.5576 ± 0.0280 | −0.0108 ± 0.0102 | 0.600 | 0.064 ± 0.006 |

A comparative examination of the linear regressions in Figure 5 and analysis of Table 4 suggest pseudo-order 1 kinetics for the oxidation reaction with Cor starch. Indeed, the coefficient of determination $R^2$ is higher for pseudo-first-order kinetics, which also has a value $[A]_{0th}$ (0.5649 ± 0.0129 mol.L$^{-1}$) close to $C_{opt} = [A]_{0exp}$ (0.6 mol.L$^{-1}$). In addition, the reaction is rapid after the first 2 hours with a half-life (Half-life $t_{1/2}$ (h)) =1.973 ± 0.135≈2h), followed by a slow stage due to the decrease in active sites and the phenomenon of diffusion. The pseudo-order 2 model seems unsuitable for describing the oxidation process because it has a low coefficient of determination and half-life $R^2$ that are incompatible with the experimental results.

**Pseudo-orders with Yam**

The linear regressions derived from the pseudo-kinetic equations applied to Yam starch are shown in Figure 6, while the corresponding parameters are summarized in Table 5.

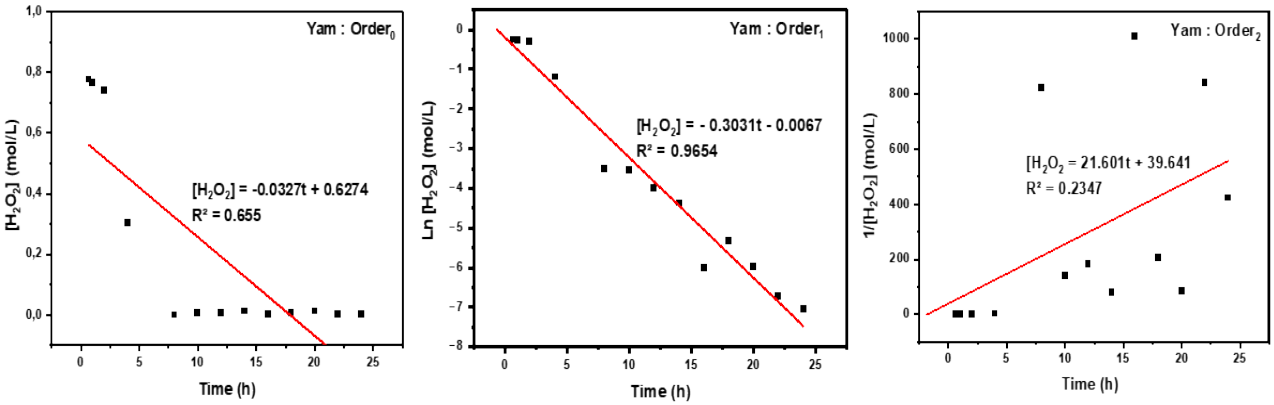


**Figure 6.** Reaction orders of Yam starch oxidation reactions.

**Table 5.** Kinetic parameters for $H_2O_2$ consumption by Yam biomass

| Order | Rate constant $k_i$ (i = 0, 1, 2) | Correlation coefficient $R^2$ | $[A]_{0th}$ (mol·L$^{-1}$) | $[A]_{0exp}$ (mol·L$^{-1}$) | Half-life $t_{1/2}$ (h) |
|---|---|---|---|---|---|
| **0** | 0.0327 ± 0.0015 mol·L$^{-1}$·h$^{-1}$ | 0.655 ± 0.013 | 0.6274 ± 0.0094 | 1.000 | 15.29 ± 0.56 |
| **1** | 0.3031 ± 0.014 h$^{-1}$ | 0.9654 ± 0.0145 | 0.9933 ± 0.0123 | 1.000 | 2.287 ± 0.105 |
| **2** | 21.601 ± 1.18 L·mol$^{-1}$·h$^{-1}$ | 0.2347 ± 0.0240 | 0.0252 ± 0.0247 | 1.000 | 0.046 ± 0.005 |

The comparative analysis of the linear regressions in Figure 6, supported by the data in Table 5, shows that the oxidation of Yam starch is best described by pseudo-order 1 kinetics. Indeed, the coefficient of

determination for pseudo-first-order kinetics is distinguished by a higher coefficient of determination ($R^2$ = 0.9654 ± 0.0145), which also has a $[A]_{0th}$ value (0.9933 ± 0.0123mol.$L^{-1}$) very close to the optimal experimental concentration $C_{opt} = [A]_{0exp}$ (1 mol.$L^{-1}$). The oxidation process is thus characterized by a rapid initial phase, observed during the first two hours and associated with a half-life $t_{1/2}$ (h) = 2.287 ± 0.105, followed by a slow stage due to the decrease in active sites and the phenomenon of diffusion. Pseudokinetics 0 and 2 do not adequately describe the system due to low coefficients of determination and half-lives that are incompatible with the experimental results.

**Pseudo-orders with Cas**

The pseudo-kinetic results for Cas starch are shown as regression lines in Figure 7, and the corresponding kinetic parameters are summarized in Table 6.

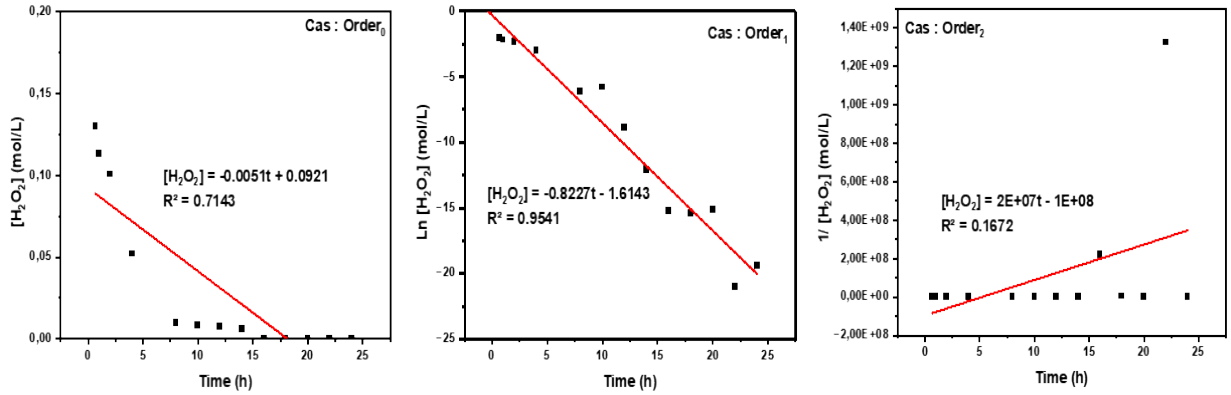


**Figure 7.** Reaction orders for starch oxidation reactions Cas.

**Table 6.** Kinetic parameter for $H_2O_2$ consumption by biomass Cas

| Order | Rate constant $k_i$ (i = 0, 1, 2) | Correlation coefficient $R^2$ | $[A]_{0th}$ (mol·$L^{-1}$) | $[A]_{0exp}$ (mol·$L^{-1}$) | Half-life $t_{1/2}$ (h) |
|---|---|---|---|---|---|
| **0** | 0.0051 ± 0.0004 mol·$L^{-1}$·$h^{-1}$ | 0.714 ± 0.023 | 0.0921 ± 0.0081 | 0.200 | 19.61 ± 1.30 |
| **1** | 0.8227 ± 0.055 $h^{-1}$ | 0.9541 ± 0.023 | 0.1990 ± 0.0160 | 0.200 | 0.843 ± 0.061 |
| **2** | 2.00 × $10^7$ ± 2.80 × $10^6$ L·$mol^{-1}$·$h^{-1}$ | 0.167 ± 0.028 | −1.00 × $10^{-8}$ ± 0.30 × $10^{-8}$ | 0.200 | 2.5 × $10^{-7}$ ± 0.5 × $10^{-7}$ |

The linear regression analysis in Figure 7, combined with the data in Table 6, shows that the oxidation of Cas starch is governed by pseudo-order 1 kinetics. Indeed, the coefficient of determination for pseudo-first-order kinetics is distinguished by a higher coefficient of determination ($R^2$ = 0.9541 ± 0.023), which also has a value $[A]_{0th}$ (0.1990 ± 0.0160 mol.$L^{-1}$) that is in excellent agreement with the experimental optimal concentration $C_{opt} = [A]_{0exp}$ (0.2 mol.$L^{-1}$). The oxidation process takes place in two successive stages: a rapid initial phase, observed during the first hour and characterized by a half-life $t_{1/2}$ (h) = 0.843 ± 0.061, followed by a slower phase attributable to the gradual decrease in active sites and diffusion limitations. The pseudo-kinetics of order 0 and 2 are clearly unsuitable for describing the system, as their low coefficients of determination and half-lives do not match the experimental results.

**Pseudo-orders with Pot**

The regression curves derived from the pseudo-kinetics of Pot starch are shown in Figure 7, and the corresponding kinetic parameters are listed in Table 7.

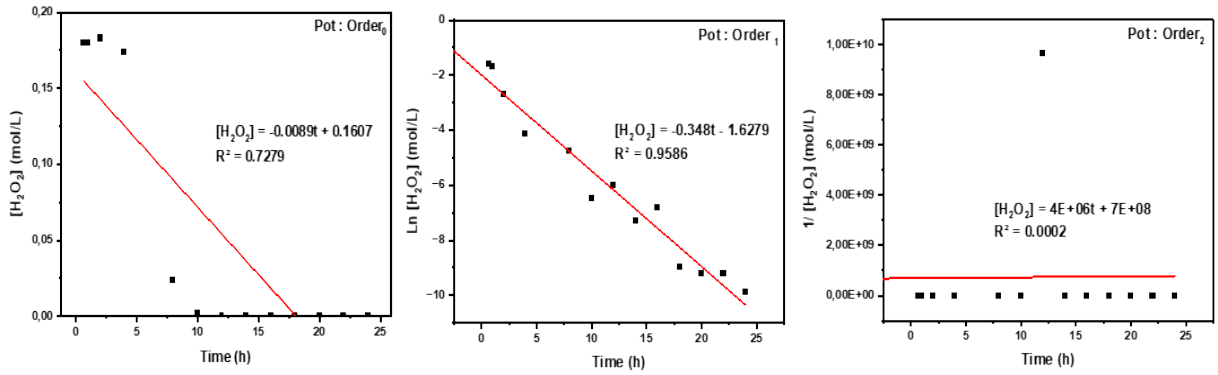


**Figure 8.** Reaction orders of starch oxidation reactions Pot.

**Table 7.** Kinetic parameter for $H_2O_2$ consumption by biomass Pot

| Order | Rate constant $k_i$ (i = 0, 1, 2) | Correlation coefficient $R^2$ | $[A]_{0th}$ ($mol \cdot L^{-1}$) | $[A]_{0exp}$ ($mol \cdot L^{-1}$) | Half-life $t_{1/2}$ (h) |
|---|---|---|---|---|---|
| **0** | 0.0089 ± 0.0007 $mol \cdot L^{-1} \cdot h^{-1}$ | 0.728 ± 0.024 | 0.1607 ± 0.0097 | 0.200 | 11.36 ± 0.52 |
| **1** | 0.348 ± 0.019 $h^{-1}$ | 0.959 ± 0.018 | 0.1963 ± 0.0088 | 0.200 | 1.99 ± 0.10 |
| **2** | $4.00 \times 10^6 \pm 0.40 \times 10^6$ $L \cdot mol^{-1} \cdot h^{-1}$ | 0.0002 ± 0.0001 | $1.43 \times 10^{-9} \pm 0.33 \times 10^{-9}$ | 0.200 | $1.25 \times 10^{-6} \pm 0.25 \times 10^{-6}$ |

The joint use of the regression lines shown in Figure 8 and the parameters reported in Table 7 leads to the conclusion that the oxidation of Pot starch preferentially follows pseudo-order 1 kinetics. Indeed, the coefficient of determination for pseudo-first-order kinetics stands out for its superior fit, with a high coefficient of determination ($R^2$ = 0.959 ± 0.018) and a value of $[A]_{0th}$ equal to 0.1963 ± 0.0088 $mol.L^{-1}$) in excellent agreement with the experimental optimal concentration $C_{opt} = [A]_{0exp}$ = 0.2 $mol.L^{-1}$. The temporal evolution of oxidation reveals two distinct phases: a rapid initial stage, observed during the first two hours and associated with a half-life $t_{1/2}$ (h) = 1.99 ± 0.10, followed by a slower phase attributable to the gradual decrease in active sites and diffusion limitations. The pseudo-kinetics of order 0 and 2 do not satisfactorily account for the behavior of the system, as their low coefficients of determination and half-lives are incompatible with the experimental results.

### 3.4. Comparison of kinetic models

The pseudo-second-order model showed poorer fit performance for all four starches, characterized by lower coefficients of determination ($R^2$) and, in some cases, theoretically calculated initial concentration values that were physically inconsistent. These results indicate that this model does not adequately describe $H_2O_2$ consumption under the experimental conditions studied. In contrast, the pseudo-first-order model generally yielded higher coefficients of determination as well as more physically consistent kinetic parameters. It was therefore selected as the most appropriate model for describing the kinetics of $H_2O_2$ consumption by the four starches.

## 4. Conclusion

In this study, the kinetics of hydrogen peroxide oxidation of starches derived from four types of biomass (Yam, Cor, Pot, and Cas) were monitored. The starches extracted from local biomass were characterized, revealing more or less compact semi-crystalline structures that may promote or limit the kinetics of oxidation. Overall, the thermal, structural, and kinetic results indicate that the $H_2O_2$ oxidation behavior of the native starches is governed by the combined effects of thermal stability, crystalline organization, granular structure, and accessibility of reactive sites. This process takes place in two successive stages: an initial rapid phase, lasting between approximately 1 and 2 hours, followed by a slower phase that continues until exhaustion. This preliminary study thus provides a relevant predictive framework for optimizing hydrogen peroxide treatment conditions, paving the way for the rational valorization of local starches and their controlled transformation into functional materials, particularly for applications in bioplastics and bio-based materials.

## Acknowledgements

The authors would like to extend their warmest thanks to the Laboratory of Environmental Thermodynamics and Physical Chemistry at Nangui ABROGOUA University in Abidjan, Côte d'Ivoire; the Department of Mathematics, Physics, and Chemistry at Peleforo GON COULIBALY University in Korhogo, Côte d'Ivoire; and the Water and Environment Laboratory of Limoges (E2Lim), UR 24133, ENSIL-ENSCI, University of Limoges, in France. Their laboratory facilities, analytical equipment, and technical assistance were essential to the success of this research.

## Author Contributions

Ouattara Taniky Sy Hamed conceived and designed the study, performed the experiments, analyzed and interpreted the data, and wrote the original draft of the manuscript. Yacouba Zoungranan supervised the research, contributed to the study design, validated the results, and critically revised the manuscript. Ekou Lynda contributed to the methodology, data analysis, and manuscript revision. Ekou Tchirioua participated in the experimental work and data collection. Kaga Taba To'ora contributed to the validation of the results and critically revised the manuscript. All authors read and approved the final version of the manuscript.

## Funding

This research received no external funding.

## Data Availability

The data supporting the findings of this study are available from the corresponding author upon reasonable request.

## Competing Interests

The authors declare no competing interests.

## References


[1] Pinto, A. M. B., Santos, T. M., Caceres, C. A., Lima, J. R., Ito, E. N., & Azeredo, H. M. C. (2015). Starch-cashew tree gum nanocomposite films and their application for coating cashew nuts. *LWT – Food Science and Technology, 62*(1), 549–554. https://doi.org/10.1016/j.lwt.2014.07.028

[2] Simões, J., Moreira, A. S. P., da Costa, E., Evtyugin, D., Domingues, P., Nunes, F. M., Coimbra, M. A., & Domingues, M. R. M. (2016). Oxidation of amylose and amylopectin by hydroxyl radicals assessed by electrospray ionisation mass spectrometry. *Carbohydrate Polymers, 148*, 290–299. https://doi.org/10.1016/j.carbpol.2016.03.034

[3] Wei, B., Li, H., Tian, Y., Xu, X., & Jin, Z. (2015). Thermal degradation behavior of hypochlorite-oxidized starch nanocrystals under different oxidized levels. *Carbohydrate Polymers, 124*, 124–130. https://doi.org/10.1016/j.carbpol.2015.01.081

[4] Debeaufort, F., Galić, K., Kurek, M., Benbettaieb, N., & Ščetar, M. (Eds.). (2021). *Packaging materials and processing for food, pharmaceuticals and cosmetics*. ISTE Ltd.; John Wiley & Sons. https://doi.org/10.1002/9781119825081

[5] Sukhija, S., Singh, S., & Riar, C. S. (2016). Effect of oxidation, cross-linking and dual modification on physicochemical, crystallinity, morphological, pasting and thermal characteristics of elephant foot yam (Amorphophallus paeoniifolius) starch. *Food Hydrocolloids, 55*, 56–64. https://doi.org/10.1016/j.foodhyd.2015.11.003

[6] Alvani, K., Qi, X., Tester, R. F., & Snape, C. E. (2011). Physico-chemical properties of potato starches. *Food Chemistry, 125*(3), 958–965. https://doi.org/10.1016/j.foodchem.2010.09.088

[7] Hamed, O. T. S., Zoungranan, Y., Lynda, E., & Tchirioua, E. (2025). Effects of controlled oxidation on the functional properties of potato, yam, cassava and corn starches. *Indian Journal of Science and Technology, 18*(6), 452–463. https://doi.org/10.17485/IJST/v18i6.3736

[8] Segal, L., Creely, J. J., Martin, A. E., & Conrad, C. M. (1959). An empirical method for estimating the degree of crystallinity of native cellulose using the X-ray diffractometer. *Textile Research Journal, 29*(10), 786–794. https://doi.org/10.1177/004051755902901003

[9] Podgorbunskikh, E., Kuskov, T., Bukhtoyarov, V., Lomovsky, O., & Bychkov, A. (2024). Recrystallization of cellulose, chitin and starch in their individual and native forms. *Polymers, 16*(7), Article 980. https://doi.org/10.3390/polym16070980

[10] Chen, Z. G., Huang, J. R., Pu, H. Y., & Keipper, H. W. (2022). The effects of temperature on starch molecular conformation and hydrogen bonding. *Starch – Stärke, 74*(3–4), Article 2100288. https://doi.org/10.1002/star.202100288

[11] Daza-Orsini, S. M., Medina-Jaramillo, C., & López-Córdoba, A. (2025). Physicochemical characterization of starch and cellulose nanofibers extracted from Colocasia esculenta cultivated in the Colombian Caribbean. *Polymers, 17*(17), Article 2354. https://doi.org/10.3390/polym17172354

[12] Pineda-Gómez, P., Angel-Gil, N. C., Valencia-Muñoz, C., Rosales-Rivera, A., & Rodríguez-García, M. E. (2014). Thermal degradation of starch sources: Green banana, potato, cassava, and corn—Kinetic study by non-isothermal procedures. *Starch – Stärke, 66*(7–8), 691–699. https://doi.org/10.1002/star.201300210

[13] Majamo, S. L., & Amibo, T. A. (2024). Study on the extraction and characterization of anchote (Coccinia abyssinica) starch and enset fiber (Ensete ventricosum) reinforced for the production of bioplastic films. *Heliyon, 10*(1), Article e23098. https://doi.org/10.1016/j.heliyon.2023.e23098

[14] Temesgen, S., Rennert, M., Tesfaye, T., Großmann, L., Kuehnert, I., Smolka, N., & Nase, M. (2024). Thermal,

morphological, and structural characterization of starch-based bio-polymers for melt spinnability. *e-Polymers, 24*(1), Article 20240025. https://doi.org/10.1515/epoly-2024-0025

[15] Kaczmarska, K., Żymankowska-Kumon, S., Byczyński, Ł., Grabowska, B., Bobrowski, A., & Cukrowicz, S. (2019). Thermoanalytical studies (TG–DTG–DSC, Py–GC/MS) of sodium carboxymethyl starch with different degrees of substitution. *Journal of Thermal Analysis and Calorimetry, 138*(6), 4417–4425. https://doi.org/10.1007/s10973-019-08892-4

[16] Kulawik-Pióro, A., Fryźlewicz-Kozak, B., Tworzydło, I., Kruk, J., & Ptaszek, A. (2025). The impact of starches from various botanical origins on the functional and mechanical properties of anhydrous lotion body bars. *Polymers, 17*(13), Article 1731. https://doi.org/10.3390/polym17131731

[17] Zhou, W., Yang, J., Hong, Y., Liu, G., Zheng, J., Gu, Z., & Zhang, P. (2015). Impact of amylose content on starch physicochemical properties in transgenic sweet potato. *Carbohydrate Polymers, 122*, 417–427. https://doi.org/10.1016/j.carbpol.2014.11.003

[18] Dome, K., Podgorbunskikh, E., Bychkov, A., & Lomovsky, O. (2020). Changes in the crystallinity degree of starch having different types of crystal structure after mechanical pretreatment. *Polymers, 12*(3), Article 641. https://doi.org/10.3390/polym12030641

[19] Kumoro, A. C., Ratnawati, R., & Retnowati, D. S. (2017). Reaction and mass transfer kinetics model of hydrogen peroxide oxidation of starch under influence of ultraviolet irradiation. *Periodica Polytechnica Chemical Engineering, 61*(3), 236–245. https://doi.org/10.3311/PPch.9354

[20] Zhou, Y., Li, X., Lv, Y., Shi, Y., Zeng, Y., Li, D., & Mu, C., (2016). Effect of oxidation level on the inclusion capacity and solution stability of oxidized amylose in aqueous solution. *Carbohydrate Polymers, 138*, 41–48. https://doi.org/10.1016/j.carbpol.2015.11.040